Hyperfine-structure studies of Zr II: Experimental and relativistic configuration-interaction results

L. Young* and C. A. Kurtz
Physics Division, Argonne National Laboratory, Argonne, Illinois 60439

Donald R. Beck and Debasis Datta
Physics Department, Michigan Technological University, Houghton, Michigan 49931
(Received 3 February 1993)

We report an experimental and theoretical study of the hyperfine structure (hfs) in various metastable levels in ^{91}Zr II. Hyperfine structures in 11 levels arising from the $4d^3$ and $4d^25s$ configurations were measured using the laser-rf double-resonance method in a collinear laser–ion-beam geometry. The hfs A and B constants were measured to a precision of 4 and 11 kHz, respectively. Less precise values for hfs constants for nine upper levels in the $4d^25p$ configuration were derived from optical spectra. Theoretically, the A and B constants for the metastable levels having $J=0.5$ and 1.5 were calculated using a relativistic configuration-interaction (RCI) approach. The final many-body wave function produced energy gaps between the five $J=0.5$ levels which differ from experiment by an average of 0.050 eV, whereas the corresponding value for the ten $J=1.5$ levels is 0.087 eV. For the two $J=0.5$ levels measured and calculated, the average error in A is 31.8%. For the three $J=1.5$ levels, the situation is better, with the average error in A being 9.2%. For comparison, the average errors in A using independent-particle Dirac-Fock (DF) wave functions were 88% and 136% for $J=0.5$ and 1.5, respectively. In all cases, the many-body (RCI) result represents a *vast* improvement from the DF result for the A values. The value for the electric-quadrupole moment of ^{91}Zr obtained from a comparison of the experimental B values and theoretical matrix elements is 0.257(0.013) b. In addition, the calculations confirm a previous report that the level at 17 614.00 cm^{-1} reported in Moore's *Atomic Energy Levels, Vol. II* (U.S. Government Printing Office, Washington, D.C., 1971) is spurious.

PACS number(s): 35.10.Fk, 32.30.Bv, 31.30.Gs, 31.30.Jv

I. INTRODUCTION

Despite the fact that a great deal of experimental [1,2] and theoretical work [3–5] has been done on the hyperfine structure (hfs) of transition-metal atoms, relatively little known about the hfs of singly charged ions. This is due in part to the difficulty of obtaining samples of ions in the perturbation-free environment necessary to study free-atom hfs. In the past several years, the application of the laser-rf double-resonance technique [6,7] to ion beams [8] has facilitated these studies, allowing us to make measurements on a wide variety of metastable states with sufficient precision to deduce both magnetic-dipole and electric-quadrupole interaction constants. Our studies initially focused on systems with two valence electrons, Sc^+ [9,10] and Y^+ [11], and, more recently we have been studying effective three-electron systems, with Ti^+ [12] and the present work on Zr^+. The recent studies are motivated by the successful many-body theoretical treatment of hfs in the two-electron systems [13], which removed the very large discrepancy between experiment and independent-particle theory. The long-term goal of these studies is to gain a predictive understanding of the many-body effects that govern hfs and other properties, e.g., oscillator strengths, in these complex systems.

Theoretically, the calculation of transition-metal electronic structure has been recognized as a challenge for well over a decade [14–17]. This is due in large part to the fact that the states in the $3d^n$, $3d^{n-1}4s$, and $3d^{n-2}4s^2$ configurations are interleaved, resulting in heavily mixed states and inequivalent radial functions for the $3d$ electrons in the differing configurations. While the above studies focused on the energetic differences, and were able to generate (in some cases) energy splittings within 0.1 eV, none calculated hfs, a very sensitive indicator of configuration interaction (CI). The earlier theoretical treatments of hfs [3,4] did not directly incorporate CI effects, but rather compared experimental values of the radial integrals to those calculated using relativistic self-consistent-field wave functions of the Hartree-Fock type in order to estimate the magnitude of these effects. In contrast, in this work, we present calculations using the relativistic CI approach [18], where many-body effects (valence-pair correlation, shallow-core–valence correlation, and core polarization) are evaluated from first principles.

The experimental results are the only measurements on hfs in the singly charged zirconium ion, although measurements have been made previously on some states in the neutral atom [19,20]. In addition, some information on hfs in doubly charged ions is available through solid-state experiments [21]. The trends shown with increasing ionization stage are now becoming apparent with the new data.

The remainder of the paper is divided into four sections. Section II describes the experimental procedure briefly. Section III gives the experimental results. Section IV outlines the relativistic CI method and compares

the experimental results and theory. Section V makes some concluding remarks.

II. EXPERIMENT

The apparatus has been described in detail before [22,10] and no essential changes were necessary for this experiment. Briefly, Zr^+ ions were produced by flowing CCl_4 over ZrO_2 in an oscillating-electron-bombardment source. The ions were extracted, accelerated to 50 keV, mass analyzed, and collimated for collinear interaction with the laser beam. There was a large component of $^{56}Fe^{35}Cl^+$ mixed with the $^{91}Zr^+$ ion of interest ($\mu = -1.3028\mu_N$, $I = \frac{5}{2}$) in the mass-analyzed beam, despite the fact that the interior source components were made of graphite and quartz. Based upon the intensity of the $m/q = 93$ peak (assigned to $^{56}Fe^{37}Cl$), we estimate that >90% of the 600-nA total beam current was actually the contaminant FeCl. This gave rise to a larger background than normal due to beam-rest gas collisions, but did not impair the experiment in a serious way.

Table I lists the 11 optical transitions studied in this experiment. While most of these transitions were chosen for accessibility, the last two entries were of special interest because the analogous levels in Ti^+ showed very large, and as yet unexplained, many-body effects in the hfs. Zr^+ ions in the metastable $4d^25s$ and $4d^3$ configurations were optically excited to the $4d^25p$ configuration with 420-nm light from a ring dye laser. The fluorescence decays to the ground configuration were detected by an EMI Model 9635QB photomultiplier tube through various combinations of wideband and interference filters. As can be seen from the table, metastable Zr^+ ions with excitations up to 20 000 cm^{-1} were formed and detected.

Figure 1 shows a representative optical spectrum of the $4d^25s\ ^2D_{5/2}$–$4d^25p\ ^4G^\circ_{5/2}$ transition. Unlike most of the optical spectra, this particular transition exhibited a

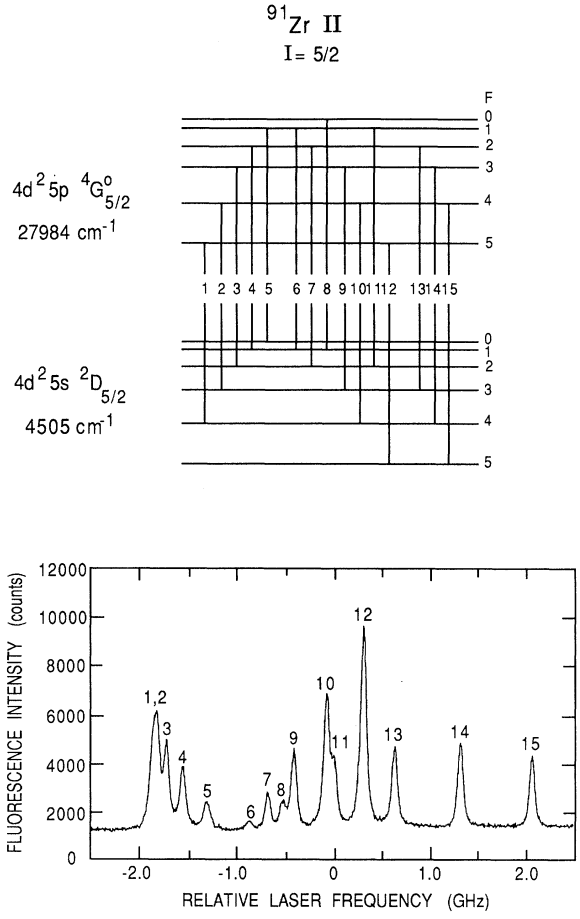

FIG. 1. A representative laser-induced fluorescence spectrum. The optical transition is from $4d^25s\ ^2D_{5/2} \rightarrow 4d^25p\ ^4G^\circ_{5/2}$. The upper portion of the figure shows the line assignments for the peaks labeled in the lower portion of the figure.

TABLE I. Optical transitions studied in $^{91}Zr^+$. The first through third columns describe the lower level and the fourth through sixth columns the upper level of the optical transitions. The last column lists the filters used to detect the fluorescence.

Lower level			Upper level			
Electron configuration	*SLJ*	Excitation energy (cm^{-1})	Electron configuration	*SLJ*	Excitation energy (cm^{-1})	Filters used
$4d^25s$	$^2D_{3/2}$	4 248.30	$4d^25p$	$^4G_{5/2}$	27 983.83	7-51
$4d^25s$	$^2D_{5/2}$	4 505.50	$4d^25p$	$^4G_{5/2}$	27 983.83	7-51
$4d^25s$	$^2F_{5/2}$	5 752.92	$4d^25p$	$^4G_{7/2}$	28 909.04	7-51
$4d^25s$	$^2F_{7/2}$	6 467.61	$4d^25p$	$^4G_{7/2}$	28 909.04	7-51
$4d^3$	$^2G_{7/2}$	7 837.74	$4d^25p$	$^4F_{5/2}$	29 504.97	7-51
$4d^3$	$^2G_{9/2}$	8 152.80	$4d^25p$	$^4F_{7/2}$	30 561.75	7-51
$4d^3$	$^4P_{1/2}$	9 553.10	$4d^25p$	$^4D_{3/2}$	32 256.71	7-51
$4d^3$	$^4P_{3/2}$	9 742.80	$4d^25p$	$^4D_{5/2}$	32 614.71	7-51
$4d^3$	$^4P_{5/2}$	9 968.75	$4d^25p$	$^4D_{7/2}$	32 899.46	7-51
$4d^3$	$^2P_{1/2}$	19 613.54	$4d^25p$	$^2D_{3/2}$	41 467.72	7-51+2800 Å
$4d^3$	$^2P_{3/2}$	20 080.30	$4d^25p$	$^2D_{5/2}$	41 676.82	7-51+2800 Å

non-standard hfs pattern and thus is reproduced here. Optical spectra were taken by scanning the dye laser under computer control and simultaneously recording fluorescence from the ion beam and transmission through a temperature-stabilized Fabry-Pérot étalon with a free spectra range of 150.00±0.01 MHz. Typically, the optical spectra had linewidths of ≈60 MHz and were taken at the lowest possible laser intensities (≤ 10 mW) to avoid power broadening. Spectra from each of the transitions listed in Table I were analyzed and used as starting points in the search for rf resonances.

rf transitions were detected in the conventional configuration, i.e., pump-rf-probe, by scanning the radio frequency applied to the resonance region and observing an increase in fluorescence in the probe region when the repopulation from a neighboring hyperfine level occurs. In the rf interaction region, the laser is also present, giving rise to possible ac Stark shifts [23]. In order to minimize these, the postacceleration voltages were selected such that the laser (power density ≤ 1 W/cm^2) was more than 2 GHz detuned from a relevant resonance in the rf region. A typical rf resonance, shown in Fig. 2, exhibits the Rabi two-level line shape and has a full width half maximum (FWHM) of approximately 500 kHz, the transit-time limit. We measured each rf resonance with the rf propagating parallel and antiparallel to the ion beam an average of 3–4 times per direction. The geometric average of the parallel and antiparallel reso-

TABLE II: Hyperfine-structure intervals from laser-rf double-resonance measurements. The first through third columns list the identifying information about the state. The fourth column lists the lower F and upper F' of the interval. The fifth and sixth columns list the observed and the fitted intervals using the A's and B's listed in Table III. The numbers in parentheses represent one standard deviation in the observed intervals. The seventh column lists the residual.

State			Interval (MHz)			
Configuration	SLJ	Energy (cm^{-1})	F-F'	Observed	Fitted	Obs.−fit (MHz)
$4d^25s$	$^2D_{3/2}$	4 248.30	3-4	803.169(13)	803.164	0.005
			2-3	594.265(10)	594.282	−0.017
			1-2	392.350(3)	392.335	0.015
	$^2D_{5/2}$	4 505.50	4-3	1685.402(3)	1685.401	0.001
			2-3	1266.628(6)	1266.632	−0.004
			1-2	845.653(6)	845.651	0.002
			0-1	423.196(4)	423.294	0.002
	$^2F_{5/2}$	5 752.92	5-4	1381.831(1)	1381.830	0.001
			4-3	1088.557(2)	1088.558	−0.001
			3-2	806.558(6)	806.557	0.001
	$^2F_{7/2}$	6 467.61	6-5	547.026(2)	547.027	−0.001
			5-4	471.524(5)	471.522	0.002
			4-3	387.471(4)	387.472	−0.001
			3-2	296.586(3)	296.586	0.000
			2-1	200.571(3)	200.572	−0.001
$4d^3$	$^2G_{7/2}$	7 837.74	6-5	207.384(5)	207.384	0.000
			5-4	149.177(3)	149.177	0.000
			4-3	103.867(2)	103.867	0.000
	$^2G_{9/2}$	8 152.80	7-6	1405.575(5)	1405.574	0.001
			6-5	1181.917(6)	1181.918	−0.001
			5-4	968.811(3)	968.813	−0.002
			4-3	764.503(5)	764.500	0.003
	$^4P_{1/2}$	9 553.10	2-3	1379.266(3)	1379.266	
	$^4P_{3/2}$	9 742.80	3-4	468.481(3)	468.480	0.001
			2-3	314.908(6)	314.908	−0.003
			1-2	192.587(2)	192.584	0.001
	$^4P_{5/2}$	9 968.65	4-5	463.082(1)	463.082	0.000
			3-4	393.669(1)	393.669	0.000
			2-3	308.785(1)	308.787	−0.002
			1-2	212.300(5)	212.303	−0.003
			0-1	108.094(5)	108.085	0.009
	$^2P_{1/2}$	19 613.54	3-2	686.228(12)	686.228	
	$^2P_{3/2}$	20 080.30	3-4	466.046(11)	466.044	0.002
			2-3	314.125(2)	314.131	−0.006
			1-2	192.568(6)	192.563	0.005

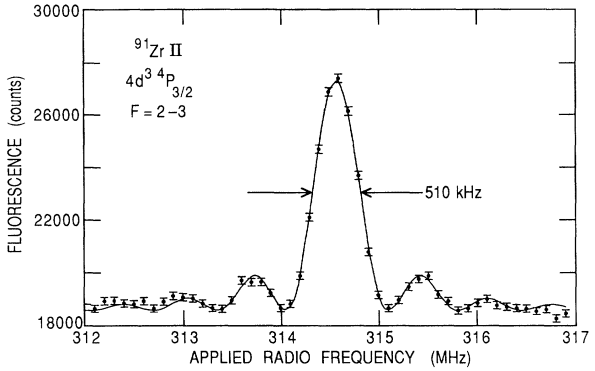

FIG. 2. A representative laser-rf double-resonance spectrum between the $F=2$ and 3 levels in the $4d^3\,^4P_{3/2}$ state. The solid line is the fit to the theoretical Rabi two-level line shape.

nance frequencies represents the true (not Doppler-shifted) interval. rf transitions were detected for all 11 metastable levels and are listed in Table II.

III. EXPERIMENTAL RESULTS AND ANALYSIS

The magnetic-dipole, A, and electric-quadrupole, B, interaction constants are determined from the standard hfs formula given by Schwartz [24]. For the lower (metastable) levels, the intervals determined by rf resonance, listed in Table II, are used in conjunction with the ordering determined by the laser-induced fluorescence spectra to determine the A's and B's. The results obtained by least-squares fitting are shown in Table III. The A and B values listed in Table III are used to calculate the intervals listed in the sixth column of Table II. The final column in Table II lists the difference between the observed and calculated hfs intervals. As can be seen from the table, the agreement between the observed and calculated intervals is excellent. Second-order corrections due to mixing of states of the same F but different J by the hyperfine interaction are too small to be observed.

For the odd-parity levels, only laser-induced fluorescence data are available. In combination with the rf data, the optical spectra were analyzed to give the A's and B's reported in Table IV. The precision for the A and B values determined this way is typically two orders of magnitude poorer than for rf data. In addition, the B values are essentially undetermined for several of the states.

IV. THEORETICAL ANALYSIS: RELATIVISTIC CI

A. Introduction

In this work, we report our first thorough relativistic many-body study of the hfs of $(d+s)^n$ levels. Except perhaps for "one-electron" ns levels, hfs routinely poses significant challenges to the theorist, due to the important contributions made from core-polarization effects [25–29] from practically all core shells. Such effects (a member of the class of "single excitations") are difficult to describe accurately due to their frequently weak coupling [30] to the zeroth-order (Dirac-Fock) solutions; many times the strongest coupling is with core–valence-pair function(s).

Many of the $(d+s)^n$ levels are energetically low lying, and can involve substantial interactions among the various components d^n, $d^{(n-1)}s$, and $d^{(n-2)}s^2$. The hfs of the d^n and $d^{(n-2)}s^2$ levels can be especially influenced by the interaction with $d^{(n-1)}s$ because (speaking nonrelativistically), the former have no zeroth-order contact hfs, whereas the latter can have a large contact contribution. Proper accounting for the energy differences of d^n and $d^{(n-1)}s$ or $d^{(n-2)}s^2$ and $d^{(n-1)}s$ can then be crucial. Doing so seems to involve the inclusion of relativistic effects from the start; these are not only associated with $d\leftrightarrow s$ substitution, which can be of the order of 0.1 eV or so [31], but also due to interactions between closely spaced levels of different L and/or S (e.g., the 22-cm^{-1} separation for Ti II $3d^3\,^2P_{1/2}$ and $3d^2 4s\,^4P_{1/2}$) [12].

From the above comments it is clear that the charac-

TABLE III. Hyperfine-interaction constants A and B derived from laser-rf double-resonance intervals listed in Table II. The first through third columns list the identifying information about the state. The fourth and fifth columns list the fitted A and B constants, respectively.

State				
Configuration	SLJ	Energy (cm^{-1})	A_{obs} (MHz)	B_{obs} (MHz)
$4d^2 5s$	$^2D_{3/2}$	4 248.30	199.2498(20)	7.706(8)
	$^2D_{5/2}$	4 505.50	−421.2272(9)	8.195(11)
	$^2F_{5/2}$	5 752.92	−272.6092(6)	−31.307(7)
	$^2F_{7/2}$	6 467.61	−94.5892(4)	39.878(4)
$4d^3$	$^2G_{7/2}$	7 837.74	−29.4056(4)	−60.181(7)
	$^2G_{9/2}$	8 152.80	−196.1072(4)	−70.336(9)
	$^4P_{1/2}$	9 553.10	459.7553(15)	
	$^4P_{3/2}$	9 742.80	110.1774(8)	34.713(3)
	$^4P_{5/2}$	9 968.65	97.7726(3)	−42.969(4)
	$^2P_{1/2}$	19 613.54	−228.7427(40)	
	$^2P_{3/2}$	20 080.30	109.7678(15)	33.716(7)

TABLE IV. Hyperfine-interaction constants A and B for upper states derived from optical spectra. The first through third columns list the identifying information about the state. The fourth and fifth columns list the fitted A and B constants, respectively.

	State			
Configuration	SLJ	Energy (cm^{-1})	A_{obs} (MHz)	B_{obs} (MHz)
$4d^2(a^3F)5p$	$^4G_{5/2}$	27 983.83	−341.0(15)	−46(12)
	$^4G_{7/2}$	28 909.04	−177.6(5)	−56(7)
	$^2F_{5/2}$	29 504.97	−223.2(12)	−2(11)
	$^2F_{7/2}$	30 561.75	−71.7(5)	−8(5)
	$^4D_{3/2}$	32 256.71	−23.9(5)	6(2)
	$^4D_{5/2}$	32 614.71	−67.6(6)	3(6)
	$^4D_{7/2}$	32 899.46	−84.5(3)	−10(4)
	$^2D_{3/2}$	41 467.72	−59.5(9)	−16(8)
	$^2D_{5/2}$	41 676.82	−156.9(52)	−17(16)

teristics of any *ab initio* theory applied to hfs of the transition metals should include the following: (i) it must be a relativistic many-body theory, (ii) it should be capable of handling the angular-momentum complexities associated with open d subshell electrons (a lot of eigenvectors and determinants are present), (iii) it should be multireference and multiroot. That is, it should treat all $(d+s)^n$ levels on an equal footing: for example, if pair correlation $4p4d \rightarrow vdvf$ is done from a $(4d_{3/2})^3$ reference function, then it must be done from all other $4d^3$, $4d^25s$, and $4d5s^2$ reference functions.

During the past few years, we have been developing a relativistic configuration-interaction (RCI) approach which we have applied to open p-shell energies and transition probabilities [32,33], and some simpler (Y II) [13] transition-metal-atom hfs. The algorithms used permitted only use of a single reference function and no more than 350 configurational functions. Additionally, angular-momentum functions involving more than 350 determinants could not be constructed. Even for the simple $(4d^2+4d5s)$ Y II case [13], these restrictions meant that a lot of core–valence-pair correlation could not be explored, and that some of the deepest core-polarization effects had to be ignored. For the current (and more complicated) species, these restrictions are so severe as to make results obtained with existing algorithms nearly meaningless. To illustrate, configurations generated from $4p^2 \rightarrow vdvf$ excitations can involve as many as 500 configurational functions and several thousand determinants. The principle three changes made to the algorithms follow. (i) We completed the implementation of the relativistic REDUCE method [33,34], whereby the original configurational functions are rotated to maximize the number of zero interactions with all reference functions (simultaneously). This method can decrease the number of configurational functions needed by an order of magnitude. (ii) We implemented the Bartlett-Condon-Beck (BCB) [35] method of constructing angular-momentum eigenstates, to avoid any limitations on the number of determinants possible. This is done by breaking up the function into two or more parts, applying the step-up and step-down operators $\mathbf{J}_\pm$ to each part (to maintain phase consistency) and then reassembling. (iii) We introduced then the Weber-Lacroix-Wanner [36] large-order multiroot diagonalization algorithm. In addition to the references cited above, further details will be given in the following paper [37].

B. Calculations

Zeroth-order wave functions are obtained by performing Dirac-Fock (DF) calculations using the program of Desclaux [38], using as a Hamiltonian a sum of one-electron Dirac operators, and the two-electron Coulomb (electrostatic) operator. Two-body relativistic effects are included from the expectation value of the Breit operator, using the zeroth-order wave functions.

Many-body effects, which are essential in this work, are included using the method of configuration interaction. It proves sufficient to restrict the many-body wave function to have a first-order form (with a few triple excitations [37]), i.e., any included configuration representing many-body effects must be related by single or double subshell excitation to one of the zeroth-order configurations: $(4d+5s)^3$ (see [33,34]). In order to have an adequately efficient methodology, fully orthonormal basis sets (both 1 and N electron) must be used throughout. This condition has been met at the zeroth-order level by generating the $1s \ldots 4p_{1/2}$, $4p_{3/2}$, $4d_{3/2}$, and $4d_{5/2}$ radial functions from a DF calculation on a single $4d^3$ level and supplying the $5s$ radial from a second DF calculation on one $4d^25s$ level. In practice this means the $4d^25s$ and to a greater extent the $4d5s^2$ zeroth-order energies, constructed from the orthonormal basis, are significantly higher than one would obtain from a DF calculation on each level. This is corrected at the many-body (CI) level, primarily through the use of symmetry preserving single excitations from both the valence $(4d, 5s)$ subshells and those of the shallow core (mainly the $4p$ subshell).

Many of the singly and doubly excited configurations are partially constructed from radial functions not present in the zeroth-order solution. We construct these functions from relativistic screened hydrogenic solutions, whose effective charge is determined during the CI process (by minimization of the energy matrix) [33,34,37]. In

this work, inclusion of s, p, d, f, and g orbital symmetries prove sufficient for the accuracies desired.

The strategy of the calculations is determined by the realization that accurate determination of the hfs of $(d+s)^n$ levels requires that energy differences be accurately described. This is done in a two-stage process [33,34,37]; in the first, valence shell many-body effects are obtained, and finally, the necessary excitations involving the core are added. Finally, the "standard" [25–29] core polarizations, necessary for accurate hfs, are introduced. For $J=0.5$, the matrix was of order ≈ 850 and for $J=1.5$, of order ≈ 1000. We anticipate matrices for $J=2.5$ and 3.5 will be somewhat larger than 1000; since our algorithms [39] are currently restricted to 1000 eigenvectors, we have not done calculations for these values of J.

C. Results and analysis

The theoretical results for fine-structure energies and the magnetic-dipole and electric-quadrupole hyperfine constants are given in Table V for $J=1.5$ and Table VI for $J=0.5$. Even though we report here only hfs constants for the measured levels (the rest will be reported elsewhere [37]), accurate determination of all the fine-structure levels of the $(d+s)^3$ complex is essential in generating good hfs results.

For $J=1.5$ the average error [40] for the nine energy differences is 705 cm^{-1} or 0.087 eV. With this work, we confirm Kiess's 1953 [41] declaration that the level published [40] at 17 614.00 cm^{-1} is spurious, and that the upper $4d^3\,^2D$ level belongs in the range 28 000–29 000 cm^{-1}. It is important to note that energy differences for all the $(d+s)^3$ levels can be determined rather accurately—contrary to the experience encountered by calculations on some highest $n(d+s)^n$ levels, where errors of up to 1 eV have been reported [17] for the location of d^n levels. One of our goals for future work will be to apply our methodology to these species, to see if we encounter such difficulties.

Although we regard the $J=1.5$ energy differences as well determined, a question remains concerning the identities of the lower $4d^3\,^2D$ and the $4d5s^2$ roots. In Table V we have presented the notation of Moore [40], even though our own analysis, Table VII, suggests the identities be reversed. Since these levels are only "split" by 869 cm^{-1} and our average error is 705 cm^{-1}, we cannot insist on the reversal. We do note that the hyperfine structure of the two levels is quite different, so a measurement, when possible, should be able to distinguish the two.

For the $J=0.5$ levels, the average error [40] in the four energy differences is 404 cm^{-1}. Although this is considerably better than for the $J=1.5$ results, the hfs constants seem not to be determined as well (see below), so perhaps a more accurate calculation of energy differences may be needed.

For $J=1.5$, the relativistic many-body magnetic-dipole hfs results (CI) of Table V exhibit an average error of 9.2% when compared with experiment. That this result is striking can be ascertained by comparing the experiment and the "DF" values (see Table V); two of the "DF" values have the wrong sign, and the third is two times larger than experiment. We should note that these "DF" values have been extracted from the CI results, and will differ "somewhat" from true DF values mainly because of coefficient changes introduced in the DF configurations by the various many-body configurations.

Results for the nuclear quadrupole moment can be obtained from Table V by dividing the experimental results by the CI value. We obtain $Q=0.244$ b ($4d^3\,^2P$), 0.260 b ($4d^3\,^4P$), and 0.267 b ($4d^2 5s\,^2D$). The average value is 0.257 b with a spread of 4–5 %. This should be compared to the value obtained by Büttgenbach *et al.* [19] of $Q=0.21(2)$ b, which does not include core-polarization

TABLE V. Fine and hyperfine structure of Zr II, $J=1.5$ $(d+s)^3$ states. The labeling of the levels (first two columns) is that given by Moore [40] as corrected by Kiess [41]. The experimental energy is also drawn from these two sources. All other quantities are from this work: the results marked CI are obtained by the relativistic many-body calculation; those marked DF are Dirac-Fock results as obtained from the CI calculations (see text).

Level		Energy (cm^{-1})		A (MHz)		[B (MHz)]/[Q(b)]	B (MHz)
Configuration	SL	Experiment	Theory (CI)	Theory	Expt.	Theory	Expt.
$4d^3$	^2D	27 699.96	29 066				
$4d^3$	^2P	20 080.30	20 710	111.5 (CI)	109.768	−138.4 (CI)	33.716
				−76.0 (DF)		−33.9 (DF)	
$4d5s^2$	^2D	14 298.64	14 996				
$4d^3$	^2D	13 428.50	14 387				
$4d^3$	^4P	9 742.80	10 072	134.1 (CI)	110.177	−133.3 (CI)	34.713
				−56.4 (DF)		−156.2 (DF)	
$4d^2 5s$	^4P	7 736.02	8 209				
$4d^2 5s$	^2P	6 111.70	6 788				
$4d^2 5s$	^2D	4 248.30	5 084	190.3 (CI)	199.250	−28.8 (CI)	7.706
				375.1 (DF)		−83.8 (DF)	
$4d^3$	^4F	2 572.21	2 950				
$4d^2 5s$	^4F	0.00	0				

TABLE VI. Fine and hyperfine structure of Zr II, $J=0.5$ $(d+s)^3$ states. The labeling of the levels (first two columns) is that given by Moore [40] as corrected by Kiess [41]. The experimental energy is also drawn from these two sources. All other quantities are from this work: the results marked CI are obtained by the relativistic many-body calculation; those marked DF are Dirac-Fock results as obtained from the CI calculations (see text).

Level		Energy (cm^{-1})		A (MHz)	
Configuration	SL	Experiment	Theory (CI)	Theory	Expt.
$4d^25s$	^2S	19477.89	20293		
$4d^3$	^2P	13889.16	14075	−143.7 (CI) −7.9 (DF)	−228.743
$4d^3$	^4P	3828.72	3628	337.5 (CI) 98.2 (DF)	459.755
$4d^25s$	^4P	1788.29	1375		
$4d^25s$	^2P	0.00	0		

effects.

For $J=0.5$, the average error in A is substantially larger, being 31.8%. Although the CI results are not as accurate as their $J=1.5$ counterparts, they offer a very great improvement over the "DF" values which are 17 $(4d^3\,^2P)$ and three $(4d^3\,^4P)$ times too small.

In Table VII we give the percent composition of each level in terms of $(4d+5s)^3$ LS states. The LS composition is determined by overlapping the final eigenvectors with LS solutions according to the prescription given in Ref. [42]. First, for all eigenvectors >91% of the weight resides in the three $(4d+5s)^3$ configurations (the rest is in the many-body configurations, whose relative weights we have not analyzed individually). Secondly, all but three of the levels have LS purities >81%; the exceptions are $4d^25s\,^4P_{3/2}$ (59%) which has a large $4s^25s\,^2P_{3/2}$ component, and $4d^3$ and $4d^25s\,^2P_{3/2}$ ($\approx$75% pure LS) which have a substantial admixture of $4d^25s\,^4P_{3/2}$. Table VII also suggests that the configuration $4d^25s$ assigned to the lower ^2P by Moore [40] might be more appropriately assigned as $4d^3$. For $J=1.5$, the upper ^2P is equally weighted between $4d^25s$ and $4d^3$ according to Table VII (Moore assigns it to $4d^3$), whereas for $J=0.5$ we would label the upper ^2P as, first, $4d^25s$. A higher degree of certainty as to whether the configurational labeling of the upper ^2P should be so J dependent would presumably occur with improvement of the $J=0.5$ hfs constants.

We next give a short list of the most important configurations; a more detailed analysis will be given elsewhere [37]. For energies, many-body configurations formed from the single excitations $4p\rightarrow p,f$ and $4d\rightarrow d$, and the doubly excited configurations (from $4d^3$) formed

TABLE VII. LS analysis (in percent) of Zr II states. The LS percentage are obtained by overlapping the CI eigenvectors with $(d+s)^3$ LS eigenvectors obtained according to the prescription of Ref. [42]. The (square of the overlap)×100% is reported in the table. We have not overlapped the CI eigenvectors with the many-body LS eigenvectors of the basis, so that the sum of the percentages across each row is less than 100%.

Level		Basis set									
		$4d^3$				$4d^25s$					$4d5s^2$
Configurations	SLJ	^2P	^4P	^2D	^4F	^2S	^2P	^4P	^2D	^4F	^2D
$4d^3$	$^2D_{3/2}$	0.0	0.006	87.72	0.005		0.0	0.007	0.204	0.0	5.030
$4d^25s$	$^2S_{1/2}$	0.039	0.003			93.71	0.171	0.073			
$4d^3$	$^2P_{3/2}$	37.29	0.089	0.460	0.0		38.50	15.48	0.003	0.192	0.0
	$^2P_{1/2}$	38.87	0.053			0.197	53.71	0.045			
$4d5s^2$	$^2D_{3/2}$	0.065	0.088	70.80	0.214		0.827	0.111	21.32	0.042	0.487
$4d^3$	$^2D_{3/2}$	0.034	0.012	8.185	0.001		0.025	0.527	16.60	0.016	65.99
$4d^3$	$^4P_{3/2}$	0.421	93.86	0.028	0.003		0.595	0.302	0.080	0.006	0.001
	$^4P_{1/2}$	0.210	95.19			0.001	0.463	0.025			
$4d^25s$	$^4P_{3/2}$	0.165	0.001	0.061	0.0		28.73	58.59	3.574	2.858	0.057
	$^4P_{1/2}$	4.236	0.003			0.058	2.155	88.68			
$4d^25s$	$^2P_{3/2}$	53.81	1.170	0.530	0.0		20.70	15.06	1.860	0.193	1.340
	$^2P_{1/2}$	52.07	0.645			0.036	36.62	6.232			
$4d^25s$	$^2D_{3/2}$	2.893	0.103	19.37	3.167		3.047	0.871	46.66	1.433	16.82
$4d^3$	$^4F_{3/2}$	0.116	0.013	1.481	92.95		0.082	0.034	1.052	0.200	0.437
$4d^25s$	$^4F_{3/2}$	0.042	0.002	0.243	0.57		0.036	2.535	1.965	89.63	0.192

from $4d^2 \rightarrow p^2+d^2+f^2$ are critical. For hfs, in addition to these, the most important are configurations generated by the excitations $4s, 5s \rightarrow s$.

Finally, it is possible to make a few general observations concerning the size of many-body effects on hfs in certain cases. For closed s-shell configurations, such as $4d^3$ and $4d5s^2$, hfs contact contributions are expected to be small at the DF level. If there is an energetically close $4d^25s$ level of the same L, S that interacts (the ^4P and ^4F matrix element between $4d^3$ and $4d^25s$ is zero; hence the weak mixing that can be seen in Table VII), then the $4d^3$ or $4d5s^2$ may "pick up" a large contact hfs from this source. We can also understand why the $4d^25s\ ^2S$ level is relatively unaffected by many-body effects. The open $5s$ dominates the hfs (the ^2S depresses orbital and spin-dipolar contributions), and additionally the level is relatively isolated. Considerations like these apply for all transition-metal atoms, and in fact we use them to help determine which levels to measure.

V. CONCLUSION

We have measured hyperfine-interaction constants for 11 levels arising from the metastable $4d^3$ and $4d^25s$ configurations in ^{91}Zr II using the laser-rf double-resonance method. Less precise values for hyperfine-interaction constants are also obtained for the upper (odd-parity) levels from the $4d^25p$ configuration. The hyperfine-interaction constants are calculated from first principles using both a many-body (RCI) and independent-particle (DF) formalism for the $J=0.5$ and 1.5 levels. Inclusion of the many-body effects improves the agreement with both experimental energy gaps and hyperfine-interaction constants in a dramatic fashion. The calculations demonstrate the capability of the relativistic configuration-interaction approach to evaluate hyperfine structure to the $\approx 10\%$ level in these complex, three-valence-electron transition-metal systems. Future studies will focus on the extension to systems with four valence electrons.

ACKNOWLEDGMENTS

We thank W. J. Childs for valuable comments and interest in this work. L.Y. wishes to thank JILA for its hospitality during the preparation of this manuscript. D.R.B. and D.D. would like to thank the Division of Chemical Sciences, Office of Energy Research, U.S. Department of Energy, Grant No. DE-FG02-92ER14282 for support of this work. This research was supported by the U.S. Department of Energy, Office of Basic Energy Science, under Contract No. W-31-109-ENG-38.

*Current address: Joint Institute for Laboratory Astrophysics, University of Colorado, Boulder, Colorado 80309.

[1] W. J. Childs, Case Stud. At. Phys. **3**, 215 (1973).
[2] S. Büttgenbach, *Hyperfine Structure in 4d- and 5d-Shell Atoms* (Springer, Berlin, 1982).
[3] G. Olsson and A. Rosén, Phys. Rev. A **25**, 658 (1982).
[4] G. Olsson and A. Rosén, Phys. Scr. **26**, 168 (1982).
[5] I. Lindgren and A. Rosén, Case Stud. At. Phys. **4**, 250 (1974).
[6] S. D. Rosner, R. A. Holt, and T. D. Gaily, Phys. Rev. Lett. **35**, 785 (1975).
[7] W. Ertmer and B. Hofer, Z. Phys. A **276**, 9 (1976).
[8] U. Nielsen, O. Poulsen, P. Thorsen, and H. Crosswhite, Phys. Rev. Lett. **51**, 1749 (1983).
[9] L. Young, W. J. Childs, T. Dinneen, C. Kurtz, H. G. Berry, L. Engstrom, and K. T. Cheng, Phys. Rev. A **37**, 4213 (1988).
[10] N. B. Mansour, T. Dinneen, L. Young, and K. T. Cheng, Phys. Rev. A **39**, 5762 (1989).
[11] T. P. Dinneen, N. Berrah Mansour, C. Kurtz, and L. Young, Phys. Rev. A **43**, 4824 (1991).
[12] N. Berrah-Mansour, C. Kurtz, L. Young, D. R. Beck, and D. Datta, Phys. Rev. A **46**, 5774 (1992).
[13] D. R. Beck, Phys. Rev. A **45**, 1399 (1992).
[14] C. Froese-Fischer, J. Phys. B **10**, 1241 (1977).
[15] C. W. Bauschlicher, J. Chem. Phys. **86**, 5591 (1987).
[16] T. H. Dunning, B. H. Botch, and J. F. Harrison, J. Chem. Phys. **72**, 3419 (1980).
[17] R. B. Murphy and R. P. Messmer, J. Chem. Phys. **97**, 4974 (1992).
[18] D. R. Beck, Phys. Rev. A **37**, 1847 (1988).
[19] S. B. Büttgenbach, R. Dicke, H. Gebauer, R. Kuhnen, and F. Traber, Z. Phys. A **286**, 125 (1978).
[20] D. S. Gough and P. Hannaford, Opt. Commun. **67**, 209 (1988).
[21] A. Abragam, J. Horowitz, and M. H. L. Pryce, Proc. R. Soc. London, Ser. A **230**, 169 (1955).
[22] L. Young, W. J. Childs, H. G. Berry, C. Kurtz, and T. Dinneen, Phys. Rev. A **36**, 2148 (1987).
[23] G. Borghs, P. DeBisschop, J. Odeurs, R. E. Silverans, and M. Van Hove, Phys. Rev. A **31**, 1434 (1985).
[24] C. Schwartz, Phys. Rev. **97**, 380 (1955).
[25] M. V. Samii, J. Andriessen, B. P. Das, S. N. Ray, T. Lee, and T. P. Das, Phys. Rev. Lett. **48**, 1330 (1982).
[26] M. V. Samii, J. Andriessen, B. P. Das, S. N. Ray, T. Lee, and T. P. Das, Phys. Rev. Lett. **49**, 1466 (1982).
[27] V. Dzuba, V. V. Flambaum, P. G. Silverstrov, and O. P. Sushkov, J. Phys. B **18**, 597 (1985).
[28] W. R. Johnson, M. Idrees, and J. Sapirstein, Phys. Rev. A **35**, 3218 (1987).
[29] A. C. Hartley and A. M. Martensson-Pendrill, Z. Phys. D **15**, 309 (1990).
[30] L. Tterlikkis, S. D. Mahanti, and T. P. Das, Phys. Rev. **176**, 10 (1968).
[31] R. L. Martin and P. J. Hay, J. Chem. Phys. **75**, 4539 (1981).
[32] Z. Cai, D. R. Beck, and W. F. Perger, Phys. Rev. A **43**, 4660 (1991).
[33] D. R. Beck and Z. Cai, Phys. Rev. A **41**, 301 (1990).
[34] D. R. Beck, Z. Cai, and G. Aspromallis, Int. J. Quantum Chem. Symp. **21**, 457 (1987).
[35] D. R. Beck, R. J. Key, A. R. Slaughter, R. D. Matthews, and M. S. Banna, Phys. Rev. A **28**, 2634 (1983).
[36] J. Weber, R. Lacroix, and G. Wanner, Comput. Chem. **4**,

55 (1980).
[37] D. R. Beck and D. Datta, Phys. Rev. A **48**, 182 (1993).
[38] J. P. Desclaux, Comput. Phys. Commun. **9**, 31 (1975).
[39] D. R. Beck, computer program RELCOR (unpublished).
[40] C. E. Moore, *Atomic Energy Levels as Derived From the Analyses of Optical Spectra,* Vol. II, Natl. Bur. Stand. (U.S.) No. NSRDS-NBS35 (U.S. GPO, Washington, DC, 1971).
[41] C. C. Kiess, J. Opt. Soc. Am. **43**, 1024 (1953).
[42] D. R. Beck, Phys. Rev. A **37**, 1847 (1988).